

# RSC Advances



This is an *Accepted Manuscript*, which has been through the Royal Society of Chemistry peer review process and has been accepted for publication.

*Accepted Manuscripts* are published online shortly after acceptance, before technical editing, formatting and proof reading. Using this free service, authors can make their results available to the community, in citable form, before we publish the edited article. This *Accepted Manuscript* will be replaced by the edited, formatted and paginated article as soon as this is available.

You can find more information about *Accepted Manuscripts* in the [Information for Authors](#).

Please note that technical editing may introduce minor changes to the text and/or graphics, which may alter content. The journal's standard [Terms & Conditions](#) and the [Ethical guidelines](#) still apply. In no event shall the Royal Society of Chemistry be held responsible for any errors or omissions in this *Accepted Manuscript* or any consequences arising from the use of any information it contains.

## ARTICLE

# Gold nanoparticles decorated on graphene-periodic mesoporous silica sandwich nanocomposite as a highly efficient and recyclable heterogeneous catalyst for catalytic applications

Cite this: DOI: 10.1039/x0xx00000x

Siyavash Kazemi Movahed, Monire Shariatipour and Minoo Dabiri\*

Received 00th January 2012,  
Accepted 00th January 2012

DOI: 10.1039/x0xx00000x

[www.rsc.org/](http://www.rsc.org/)

The ultra-small Au nanoparticles (Au NPs) immobilized HS-functionalized sandwich-like periodic mesoporous silica (PMS) coated graphene (G) to form a novel nanocomposite catalyst Au NPs@HS-G-PMS. The synthesized Au NPs@HS-G-PMS nanocatalyst exhibited excellent catalytic activity on the three kinds of organic reactions. The reduction of 4-nitrophenol by sodium borohydride, the Suzuki-Miyaura cross coupling reaction of aryl halides with phenyl boronic acid and three coupling reaction of aldehyde, alkyne, and secondary amine ( $A^3$ -coupling) in water were successfully done. Most importantly, the catalyst could be used repetitively more than six times without significant deactivation.

## Introduction

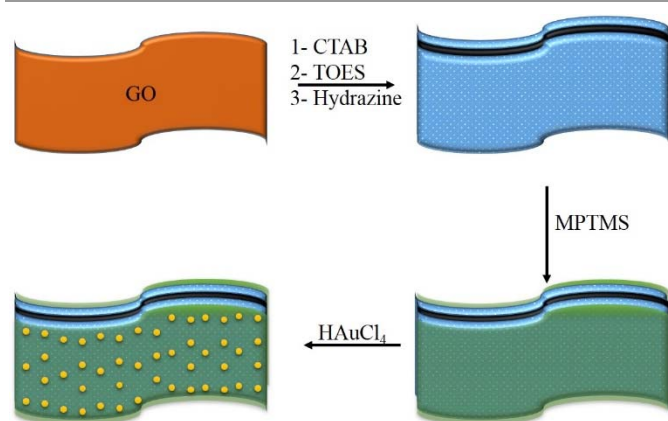
Recently, graphene which is a single layer of  $sp^2$  carbon atoms bonded in a hexagonal lattice has attracted great attention from scientists all over the world. The extraordinary properties of these exfoliated graphene sheets, such as their extremely large surface area,<sup>1</sup> fast charge mobility,<sup>2</sup> remarkably high mechanical strength and Young's modulus,<sup>3</sup> excellent chemical stability<sup>4</sup> and low manufacturing cost make graphene a promising candidate to disperse or immobilize catalytically active species for heterogeneous catalysis.<sup>5</sup> Graphene supported metal nanoparticles (NPs) composites have been widely studied, and a strong metal-graphene interaction was also revealed and may contribute to the enhanced catalytic performance of the supported metal NPs.<sup>6</sup>

The periodic mesoporous silica-coated graphene (G-PMS) hybrids have shown great capabilities to circumvent the known limitations of the applications of most graphene-supported metal nanocatalysts.<sup>7</sup> The aggregation of graphene sheets would be avoided due to the restraining of the  $\pi$ - $\pi$  stacking interactions by amorphous PMS external layer. In addition, owing to have a substantial number of mesopores, the PMS layers can confine metal nanoparticles selectively based on their specific size. The confinement in PMS and generally porous materials can prevent metal nanoparticles from sintering into the larger clusters, which happen under harsh reaction conditions such as at high temperatures required for many catalytic and detoxification processes. Therefore, novel methods to secure ultrafine metal nanoparticles (<2 nm) onto graphene supports have been devised

while enhancing the dispersibility and stability of graphene-supported metal nanocatalysts, which lead to preservation of catalytic activity even under harsh reaction conditions.<sup>8</sup>

As shown in Scheme 1, G-PMS were synthesized through combining sol-gel and *in situ* reduction techniques. The 2D sandwich-like graphene-based periodic mesoporous silica (G-PMS) hybrids were prepared via soft template-assisted reducing process. In this procedure, the cationic surfactant cetyltrimethylammonium bromide (CTAB) was chosen to electrostatically adsorb and self-assemble onto the surface of highly negatively charged graphene oxide in alkaline solution. Upon hydrazine reduction treatment and the soft-template removing, the G-PMSs products were successfully collected with mesoporous silica around the surface of single-layer graphene oxide.<sup>9</sup> PMS covered on the surface of G could act as a stabilizing agent to prevent serious aggregation of individual G by weakening the  $\pi$ - $\pi$  stacking interaction between G nanosheets. Then, the hydroxyl groups of G-PMS were converted to -SH groups by a silylation modification technique on G-PMS with 3-mercaptopropyltrimethoxysilane (MPTMS). The metal affinity groups, such as  $NH_2$ ,  $SiH$ , SH groups have been post-grafted onto the surface of catalyst support to stabilize and prevent the metal nanoparticles from aggregating.<sup>10</sup> Among them, SH group bind to gold surfaces with high affinity, most frequently thiol modified ligands are used as stabilizing agents which bind to the surface of the AuNPs by formation of Au-sulfur bonds.<sup>11</sup> Finally, the immobilization of ultra-small and well dispersed Au NPs on the surface of G-PMS was conducted

via an *in situ* reduction of  $\text{HAuCl}_4$  as the precursor to yield the Au NPs@HS-G-PMS hybrid.



**Scheme 1.** Schematic diagram illustrating the synthesis of Au NPs@HS-G-PMS nanocatalyst

## Experimental section

### Chemicals

All chemicals were purchased from commercial suppliers and all solvents were purified and dried using standard procedures.

### Physical measurements

XPS analysis was performed using a Gamdata-scienta ESCA 200 hemispherical analyzer equipped with an Al K $\alpha$  (1486.6 eV) X-ray source. Raman spectra of G-PMS, HS-G-PMS, and Au NPs@HS-G-PMS hybrids were recorded on a Bruker SENTERR (2009) with an excitation beam wavelength at 785 nm. Scanning electron microscope G-PMS, HS-G-PMS, and Au NPs@HS-G-PMS hybrids were performed using Hitachi S-4160 SEM and Philips XL-30 ESEM. Diffraction data were collected on two STOE STADI P reflection and transmission mode and Cu-K $\alpha$ 1 radiation ( $\lambda = 1.5406 \text{ \AA}$ ). Transmission Electron Microscopy characterization of G-PMS and Au NPs@HS-G-PMS hybrids fresh and reused nanocomposites were performed using a transmission microscope Philips CM-30 with an accelerating voltage of 150 kV. Melting points of products were measured on an Electrothermal 9100 apparatus and are uncorrected. The concentration of gold was estimated using Shimadzu AA-680 flame atomic absorption spectrophotometer and inductively coupled plasma optical emission spectrometer (ICP-OES) Varian Vista PRO Radial. The thermal stability of the G-PMS, HS-G-PMS, and Au NPs@HS-G-PMS hybrids were determined using a thermogravimetric analyzer (TGA/DTA Bahr: STA 503) under air and a heating rate of  $10 \text{ }^\circ\text{C min}^{-1}$ . Elemental analysis of HS-G-PMS hybrid was performed using an Elementar Analysensysteme GmbH VarioEL CHNS. The nitrogen adsorption-desorption isotherms of G-PMS, HS-G-PMS, and Au NPs@HS-G-PMS hybrids were collected by using a Micrometrics PHS-2828(PHSCINA) surface area analyser with  $\text{N}_2$  at 77.3 K. UV/Vis spectra were recorded employing an Analytik Jena Specord S600 Diode Array spectrometer. Gas

chromatography was performed on a Trace GC ultra from the Thermo Company equipped with FID detector and Rtx®-1 capillary column.

### Preparation of Graphene Oxide

The graphite powder (2.5 g) was first treated with a mixture of 12.5 mL of concentrated  $\text{H}_2\text{SO}_4$  with 2.5 g  $\text{K}_2\text{S}_2\text{O}_8$  and 2.5 g  $\text{P}_2\text{O}_5$ . The mixture was kept at  $80 \text{ }^\circ\text{C}$  for 6 h. Subsequently, the mixture was cooled to room temperature and diluted with 500 mL DI water and left overnight. The mixture was then filtered and washed with DI water to remove the residual acid. The product was dried under ambient conditions overnight. The pre-oxidized graphite was then subjected to oxidation by Hummers's method. The pretreated graphite powder was put into cold ( $0 \text{ }^\circ\text{C}$ ) concentrated  $\text{H}_2\text{SO}_4$  (125 mL). Then  $\text{KMnO}_4$  (15 g) was added gradually under stirring, and the temperature of the mixture was kept below  $20 \text{ }^\circ\text{C}$  by cooling. The mixture was then stirred at  $35 \text{ }^\circ\text{C}$  for 4 h and then diluted with DI water (250 mL). Because adding water to concentrated sulfuric acid medium releases a large amount of heat, the dilution was carried out in an ice bath to keep the temperature below  $50 \text{ }^\circ\text{C}$ . After adding all of the 250 mL DI water, the mixture was stirred for 2 h, and then an additional 750 mL DI water was added. Shortly thereafter, 20 mL 30%  $\text{H}_2\text{O}_2$  was added to the mixture and the colour of the mixture changed into brilliant yellow and began bubbling. The mixture was filtered and washed with 0.5 M HCl to remove metal ions, followed by 500 mL DI water to remove the acid, and then was dialyzed against DI water. The resulting GO solid was dried in air.<sup>12</sup>

### Preparation of G-PMS

79 mL the as-synthesized GO ( $3.8 \text{ mg mL}^{-1}$ ) aqueous solution was added into 602 mL water containing 6.8 g CTAB and 0.27 g NaOH, and then ultrasonically treated for 2 h. After magnetic stirring for 2 h at  $40 \text{ }^\circ\text{C}$ , tetraethylorthosilicate (TEOS; 5.4 mL dissolved in 21.7 mL ethanol) was slowly added to the above mixture. After reaction for 12 h, 1.8 mL of hydrazine was additionally introduced into the above mixture, and then heated at  $70 \text{ }^\circ\text{C}$  for 5 h. The obtained product was centrifuged and washed with warm ethanol for three times. The product was then dispersed in 680 mL acetone stirred at  $40 \text{ }^\circ\text{C}$  for 24 h. The product was collected by centrifugation and washed by warm ethanol for three times.<sup>9</sup>

### Preparation of HS-G-PMS

The (0.1 g) was ultrasonically dispersed in 630 mL of ethanol. Then, solution of MPTMS (2 mmol in 50 mL ethanol) was added to the G-PMS suspension under stirring, and refluxed for 12 h. The yielded suspension was centrifuged and washed with ethanol for several times to get a purified HS-G-PMS. The loading of sulfur was determined to be 4.85 wt% from elementary analysis (CHN).

### Preparation of Au NPs@HS-G-PMS

The HS-G-PMS (0.2 g) was ultrasonically dispersed in 100 mL of DI  $\text{H}_2\text{O}$ . Then, 0.52 mL of  $\text{HAuCl}_4$  (0.04 M) was added to the

RGO suspension under stirring. The mixture was kept at room temperature for 5 h with constant stirring. The resulted precipitation was collected and repeated washing with DI H<sub>2</sub>O and Ethanol, and dried at room temperature. The ICP analysis gave the actual Au contents as 1.8 wt.% for Au NPs-RGO hybrid.

#### General procedure for the reduction of 4-NP

The reduction of 4-NP by NaBH<sub>4</sub> was chosen as a model reaction to investigate the catalytic performance of the Au NPs@HS-G-PMS hybrid. In short, 30 mL of 4-NP (0.12 mM) were mixed with 30 mL of a freshly prepared aqueous NaBH<sub>4</sub> solution (0.17 M). Then, hybrid (0.25 mol% of Au) was added to the resulting solution, and the reaction was allowed to proceed until the solution became colorless. The reaction conversion was determined by ultraviolet visible spectroscopy (UV-Vis).

#### General procedure for Suzuki reaction

A mixture of Au NPs@HS-G-PMS hybrid (2 mol % of Au), K<sub>3</sub>PO<sub>4</sub> (3 mmol), aryl halides (1.0 mmol), phenyl boronic acid (1.2 mmol), and H<sub>2</sub>O (3 mL) under air was stirred for 6 h at 100 °C. The reaction progress was monitored by GC. After completion of the reaction, the heterogeneous mixture was cooled to room temperature and the catalyst was separated from reaction medium simple filtration. Then, the reaction mixture was concentrated and then residue was purified by column chromatography (SiO<sub>2</sub>, *n*-Hexane and Ethyl acetate) to yield pure product. The catalysts were recovered by using a simple filtration and washed extensively with acetone and deionized water and drying in the air.

#### General procedure for A<sup>3</sup>-coupling reaction

A mixture of Au NPs@HS-G-PMS hybrid (7.5 mol % of Au), aldehyde (1.0 mmol), amine (1.2 mmol), acetylene (1.3 mmol) in H<sub>2</sub>O (3 mL) was refluxed at 100 °C for 24 h. After completion of the reaction (TLC), the heterogeneous mixture was cooled to room temperature and the catalyst was separated from reaction medium simple filtration. Then, the reaction mixture was concentrated and then residue was purified by column chromatography (SiO<sub>2</sub>, *n*-Hexane and Ethyl acetate) to yield pure product. The catalysts were recovered by simple filtration and washed extensively with acetone and deionized water and drying in the air.

All products are known compounds and were reported previously.

## Results and discussion

### Characterization

Raman spectroscopy is a very useful tool for investigating the electronic and phonon of structure graphene-based materials.<sup>13</sup> The Raman spectra of the prepared G-PMS, HS-G-PMS, and Au NPs@HS-G-PMS hybrids are shown in Fig. 1. The characteristic D and G bands of carbon materials are observed around 1300 and 1600 cm<sup>-1</sup>, respectively. The D band is characteristic of a breathing mode for k-point phonons of A<sub>1g</sub>, while the G band is

the result of the first-order scattering of the E<sub>2g</sub> mode of sp<sup>2</sup> carbon domains.<sup>14</sup> The intensity ratio of D and G peaks, I<sub>D</sub>/I<sub>G</sub>, is used as a measure of the disorder or restoration of the graphene lattice and expressing the sp<sup>2</sup>/sp<sup>3</sup> carbon ratio.<sup>15</sup> As shown, after the silylation of G-PMS with MPTMS, the I<sub>D</sub>/I<sub>G</sub> was 1.95 for the resulting HS-G-PMS, while the it was 1.85 for G-PMS. Considering the G band and D band that represent the sp<sup>2</sup> and sp<sup>3</sup> C atoms, respectively, it can be anticipated that the increasing of the sp<sup>3</sup> hybridization structure (MPTMS) raises from the successful silylation modification. The I<sub>D</sub>/I<sub>G</sub> decreases to 1.45 for the Au NPs@HS-G-PMS, possibly as a result of the Au NPs growth at defective regions of the HS-G-PMS surface.<sup>16</sup> Additionally, after conjugation of the Au NPs onto the HS-G-PMS sheets, the intensity of the Raman signals of graphene (D and G bands) were enhanced relative to HS-G-PMS, because of the surface enhanced Raman spectroscopy (SERS) of Au NPs. SERS were obtained *via* an electromagnetic enhancement (excitation of localized surface plasmons involving a physical interaction) or chemical enhancement (formation of charge-transfer complexes involving chemical interaction) with enhancement factors of ~10<sup>12</sup> and ~10 to 100, respectively. The low enhancement factor for the Au NPs@HS-G-PMS hybrid indicates the presence of a chemical interaction or bonding between Au NPs and HS-G-PMS.<sup>17</sup>

The electronic properties of hybrid were probed by X-ray photoelectron spectroscopy (XPS) analysis. As shown in Fig. 2, the peaks corresponding to Au 4f, Si 2p, S 2p, C 1s and O 1s are clearly observable in the XPS full spectrum. The XPS spectrum of Au 4f core for Au NPs@HS-G-PMS level displays main peaks at 84.18 and 87.81 eV which correspond to the binding energy of Au<sup>0</sup> 4f<sub>7/2</sub> and Au<sup>0</sup> 4f<sub>5/2</sub>, respectively (Fig. 2b).<sup>18</sup> A pronounced peak at 101.91 eV (in the Si 2p XPS spectrum) which corresponds to the bonding energy of Si–O–C can be easily observed.<sup>19</sup> The S 2p signal for Au NPs@HS-G-PMS hybrid includes two components. The first constitutes two doublets, situated at 162.24 and 162.93 eV, respectively, attributable to S–Au groups on G-PMS sheets. The second component located at 163.48 and 164.36 eV is attributable to the sulfur atoms of the SH groups.<sup>20</sup>

The microstructure and morphology of the hybrids are characterized by means of scanning electron microscopy (SEM) and transmission electron microscopy (TEM). As is seen in representative SEM micrographs (Fig. 3 a-f), G-PMS, HS-G-PMS, and Au NPs@HS-G-PMS hybrids remain as a nanosheet-like structures, with lateral dimensions ranging from hundreds of nanometers to a few microns. Additionally, the SEM micrographs of G-PMS, HS-G-PMS (Fig. 3 a-d) show increasing layer thickness by addition of MPTMS to G-PMS surface. Additionally, the density and distribution of elements of the Si, S, and Au on the Au NPs@HS-G-PMS hybrid are evaluated by quantitative energy dispersive X-ray spectroscopy (EDS) mapping (Fig. 4b-d).

Fig. 5 a-d compares the morphologies of G-PMS and Au NPs@HS-G-PMS, as investigated by TEM. The micrograph of G-PMS possesses similar sheet morphology (Fig. 5a-b). As Fig.

4c-d shows, the surfaces of HS-G-PMS are covered with good dispersion of Au NPs with an average size of  $\sim 2$  nm.

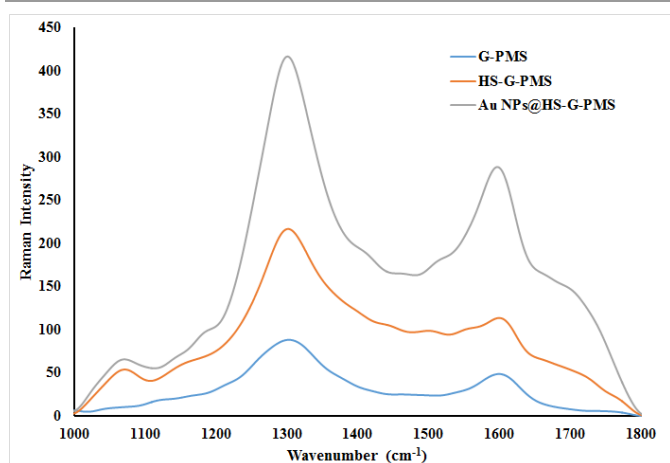


Fig. 1 Raman spectra G-PMS, HS-G-PMS, and Au NPs@HS-G-PMS hybrids

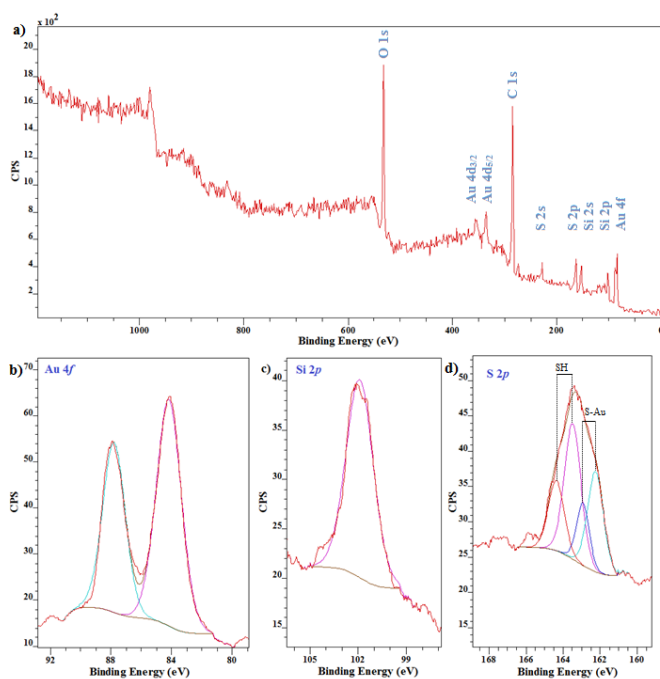


Fig. 2. (a) Full range XPS spectrum of Au NPs@HS-G-PMS hybrid. (b) Au 4f, (c) Si 2p, and (d) S 2p core level regions XPS spectra of Au NPs@HS-G-PMS hybrid, respectively

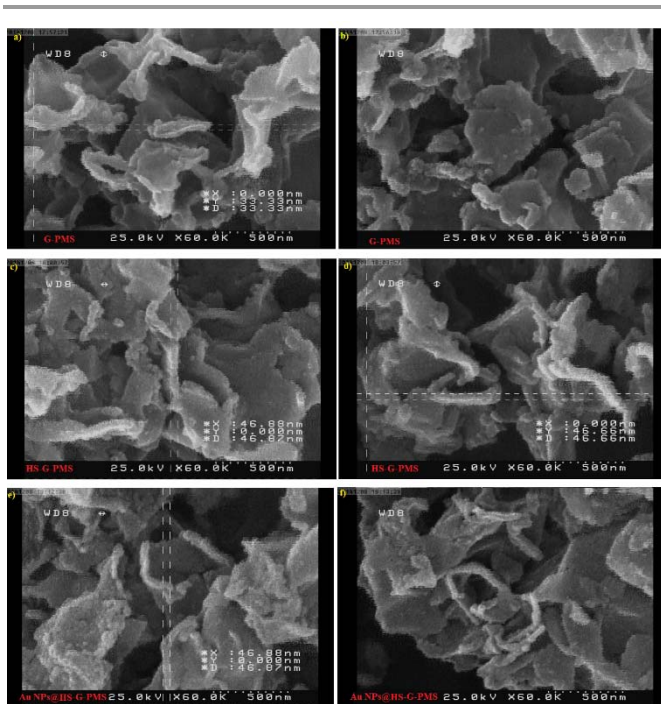


Fig. 3 SEM micrographs of (a-b) G-PMS, (c-d) HS-G-PMS and (e-f) Au NPs@HS-G-PMS hybrids

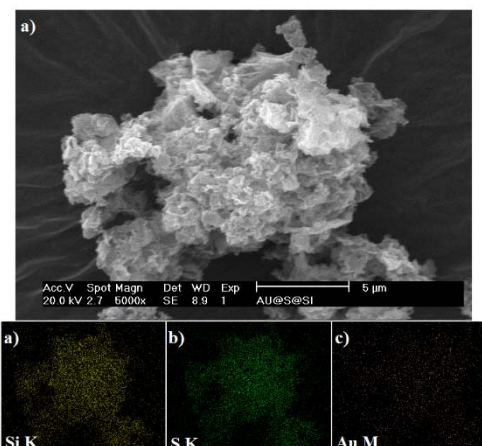


Fig. 4 SEM micrograph of (a) Au NPs@HS-G-PMS hybrids and corresponding quantitative EDS element mapping of (b) Si, (c) S and (d) Au.

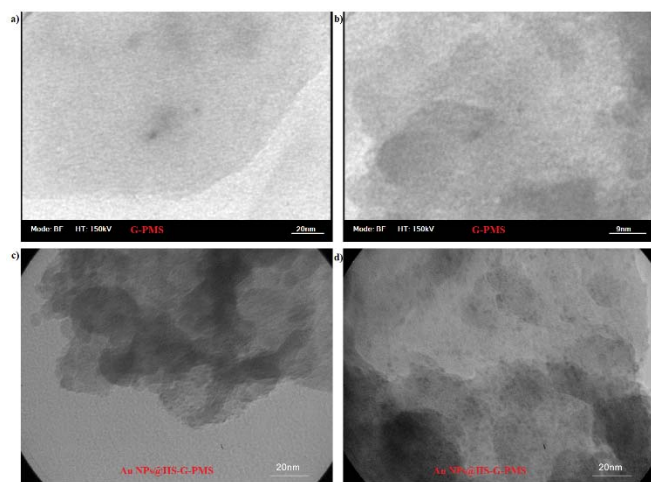


Fig. 5 TEM micrographs of (a-b) G-PMS, and (c-d) Au NPs@HS-G-PMS hybrids

The porous nature of G-PMS, HS-G-PMS, and Au NPs@HS-G-PMS hybrids was evaluated by nitrogen physisorption measurements. The specific surface area was calculated from the adsorption isotherms based on the Brunauer–Emmett–Teller (BET) analysis. It was found that the isotherms of G-PMS, HS-G-PMS, and Au NPs@HS-G-PMS hybrids are type IV according to the IUPAC classification, associated with a well-defined capillary condensation step suggesting a mesoporous structure.<sup>21</sup> The BET total surface areas of G-PMS, HS-G-PMS, and Au NPs@HS-G-PMS hybrids were found to be 452.86, 615.43 and 648.59 m<sup>2</sup>g<sup>-1</sup>, respectively (Fig. 6a). From these results, it can be concluded that the MPTMS and Au NPs act as spacers between G-PMS sheets thereby preventing their agglomeration and aggregation.<sup>22</sup> Moreover, the volume adsorbed was larger at high relative pressure, exhibiting the H3-type hysteresis loop, and this kind of hysteresis loop indicated that these hybrids are comprised of aggregates of plate-like particles forming slit-like pores.<sup>23</sup> The average pore size diameters of G-PMS, HS-G-PMS, and Au NPs@HS-G-PMS were calculated to be 2.48, 2.55 and 2.58 nm, respectively, using Barrett-Joyner-Halenda (BJH) analysis.

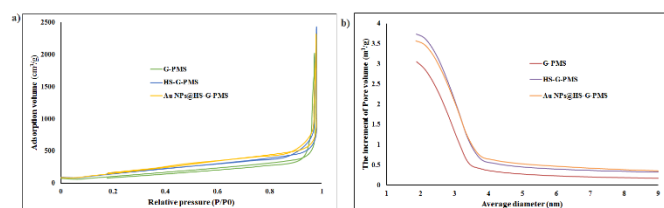


Fig. 6 (a) Nitrogen adsorption–desorption isotherms of G-PMS, HS-G-PMS, and Au NPs@HS-G-PMS hybrids (b) the pore size distribution curves of G-PMS, HS-G-PMS, and Au NPs@HS-G-PMS hybrids

Thermogravimetric analysis (TGA) was further used to study the thermal behavior and stability of the Au NPs@HS-G-PMS hybrid. TGA plots of GO, G-PMS, HS-G-PMS, and Au NPs@HS-G-PMS hybrids are shown in Fig. 7. The weight of GO declined sharply between 100 °C and 200 °C, due to pyrolysis of the labile oxygen-containing functional groups. Since SiO<sub>2</sub> is

resistant to high temperature, G-PMS is thermally stable compared with GO and had a little weight loss indicating SiO<sub>2</sub> was successfully coated onto GO. The total weight lost for G-PMS, HS-G-PMS, and Au NPs@HS-G-PMS hybrids were only 42.20, 23.32 and 21.26% at temperatures around 450 °C, respectively.

The XRD pattern of the Au NPs@HS-G-PMS hybrid is shown in Fig. 8. The diffractions for the Au crystal are hardly detected, resulting from the small size of Au NPs.<sup>24</sup> The G-PMS hybrid showed diagnostic diffraction peak with *d* spacing around 4.82 nm. It is assigned to *d*<sub>100</sub> XRD reflection from hexagonally ordered PMS.<sup>25</sup> The peaks at 2θ=44 and 64 degrees correspond to stainless steel sample holder of powder diffractometer.

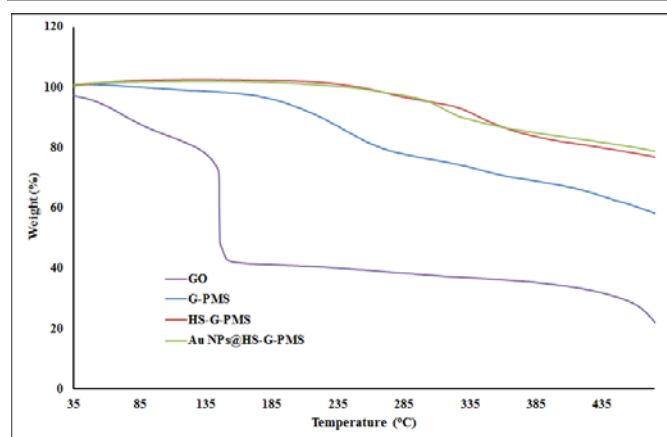


Fig. 7 TGA plots of GO, G-PMS, HS-G-PMS, and Au NPs@HS-G-PMS hybrids

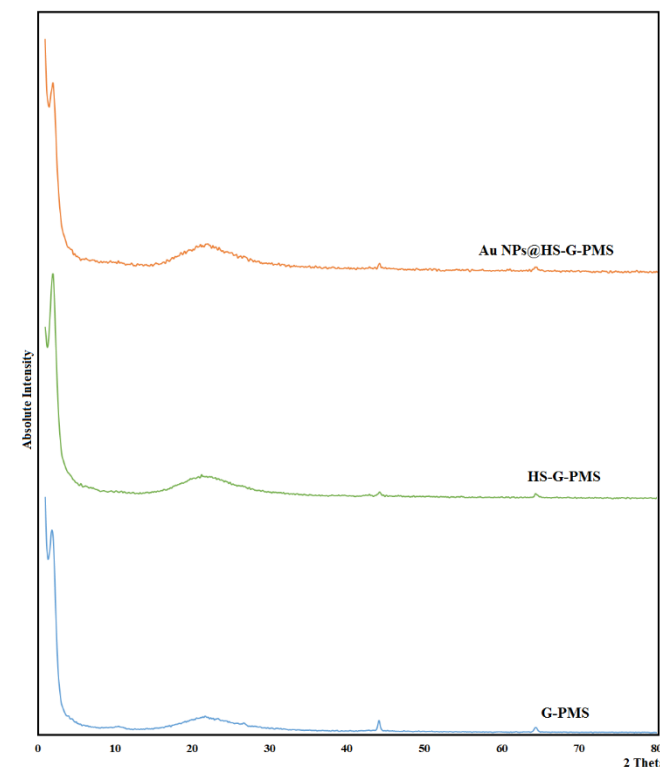
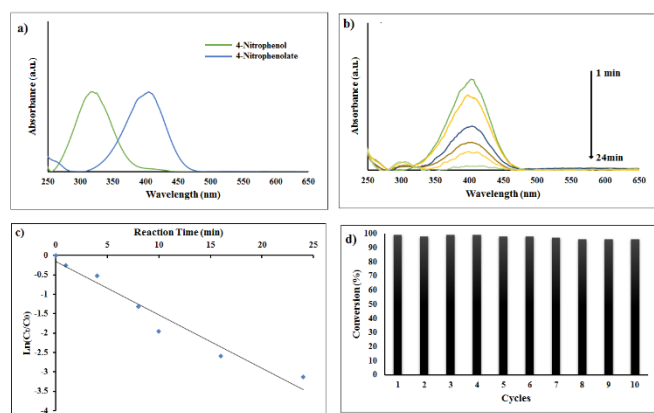


Fig. 8 XRD patterns of GO, G-PMS, HS-G-PMS, and Au NPs@HS-G-PMS hybrids.

## The catalytic activity of Au NPs@HS-G-PMS hybrid toward the reduction of 4-nitrophenol by sodium borohydride

After the careful investigation of the prepared Au NPs@HS-G-PMS hybrid, it was employed in the catalytic reduction of 4-nitrophenol (4-NP) in the presence of NaBH<sub>4</sub> as a hydrogen source, because Au NPs are known to be effective in the conversion of 4-NP. As is well known, 4-nitrophenol (4-NP), a well-characterized industrial pollutant that has been listed on the “Priority Pollutant List” by the U.S. Environmental Protection Agency, is harmful to aquatic life and human health in terms of its toxicity, potential carcinogenicity, and mutagenicity.<sup>26</sup> Hydrogenation of 4-NP to the corresponding 4-aminophenol (4-AP) is known as one of the fundamental reactions for the synthesis and manufacture of fine and industrial chemicals for the production of analgesic and antipyretic drugs, photographic developer, corrosion inhibitor, anticorrosion lubricant, and soon.<sup>27</sup>

As shown in Fig. 9a, the pure of 4-NP solution exhibited a distinct absorption maximum at 317 nm, which shifts to 400 nm in the presence of an alkali because of the formation of 4-nitrophenolate ion. It was found that the intensity of the characteristic absorption peak of 4-nitrophenolate ion at 400 nm quickly decreases, and the characteristic absorption of 4-AP at around 300 nm also appears rapidly (Fig. 9b). The reaction kinetic could be analyzed and confirmed from the time-dependent absorption spectra, which showed the gradually decrease of 4-nitrophenolate ions. Linear relationships between  $\ln(C_t/C_0)$  and reaction time were obtained in the reduction reaction catalyzed by Au NPs@HS-G-PMS hybrid, which match well with the first-order reaction kinetics. The rate constant  $k$  was calculated to be 0.14 min<sup>-1</sup> for the reaction catalyzed by Au NPs@HS-G-PMS hybrid (Fig. 9c). The recyclability of the Au NPs@HS-G-PMS hybrid was also examined by the reduction of 4-nitrophenol. It was found that the recovery can be successfully achieved in ten successive reaction runs (Fig. 9d).



**Fig. 9** (a) UV-vis spectra of (a) 4-nitrophenol and 4-nitrophenolate; (b) the reduction of 4-NP to 4-AP over Au NPs@HS-G-PMS hybrid; (c) plot of  $\ln(C_t/C_0)$  against the reaction time of the reduction of 4-NP over Au NPs@HS-G-PMS hybrid; (d) the catalytic stability tests of Au NPs@HS-G-PMS hybrid.

## The catalytic activity of Au NPs@HS-G-PMS hybrid toward the Suzuki–Miyaura cross-coupling reaction

Aryl–aryl bond formation via the palladium-catalyzed Suzuki cross coupling reaction is one of the most important tools of modern organic synthesis. The Suzuki cross coupling reaction is one of the most general and powerful tools for the synthesis of pharmaceuticals, herbicides, polymers, liquid crystals, natural products, ligands for catalysis and advanced materials.<sup>28</sup>

Inspired by the high activity and stability of Au NPs@HS-G-PMS hybrid, the Suzuki coupling reaction was further employed as another model reaction to test the further performance of Au NPs@HS-G-PMS nanocatalyst. We chose the Suzuki–Miyaura coupling reaction of phenyl boronic acid with phenyl iodide as a model reaction in H<sub>2</sub>O as solvent at 100 °C in the presence of K<sub>3</sub>PO<sub>4</sub> as base and with a catalyst loading of 2 mol% of Au for 6 h. Under this condition, we found that the cross coupling reaction proceeds well, affording the excellent yield (93%) of the corresponding biphenyl.

We next managed to examine the scope and limitation of Suzuki–Miyaura reaction with various types of aryl halides derivatives and phenyl boronic acid. (Table 1). It can be seen from Table 1 that the Suzuki–Miyaura cross-coupling reaction with most substrates preceded in good yields. Aryl iodides and bromides bearing electron-donating and electron-withdrawing groups reacted well giving good yields. The hindered substrates such as 2-iodotoluene and 2-iodo-1,3,5-trimethylbenzene converted into the corresponding products with a moderate yield (Table 1, entries 7 and 8).

**Table 1** Au NPs@HS-G-PMS hybrid catalyzed Suzuki–Miyaura cross-coupling reaction<sup>a</sup>

Ar <sup>1</sup> -X + Ph-B(OH) <sub>2</sub> → Ar <sup>1</sup> -Ph			
Entry	Ar <sup>1</sup>	X	Yield <sup>b</sup>
1	Ph	I	93%
2	4-Me-C <sub>6</sub> H <sub>4</sub>	I	87%
3	4-MeO-C <sub>6</sub> H <sub>4</sub>	I	84%
4	4-NO <sub>2</sub> -C <sub>6</sub> H <sub>4</sub>	I	95%
5	4-MeCO-C <sub>6</sub> H <sub>4</sub>	I	96%
6	4-CO <sub>2</sub> H-C <sub>6</sub> H <sub>4</sub>	I	91%
7	2-Me-C <sub>6</sub> H <sub>4</sub>	I	76%
8	Ph	I	58%
9	1,3,5-Trimethyl-C <sub>6</sub> H <sub>2</sub>	I	58%
10	4-Me-C <sub>6</sub> H <sub>4</sub>	Br	83%
11	4-NO <sub>2</sub> -C <sub>6</sub> H <sub>4</sub>	Br	89%

<sup>a</sup> Aryl halide (1 mmol), phenyl boronic acid (1.2 mmol), Au NPs@HS-G-PMS (2 mol % of Au), K<sub>3</sub>PO<sub>4</sub> (3 mmol), 100 °C, 6h. <sup>b</sup> Isolated yield.

The reusability of the Au NPs@HS-G-PMS hybrid was examined in Suzuki–Miyaura cross-coupling reaction of phenyl boronic acid with phenyl iodide. It was found that the recovery can be successfully achieved in six successive reaction runs (Table 2). The heterogeneous nature of the catalysis was proved using a hot filtration test and atomic absorption spectroscopy (AAS) analysis. To determine whether the catalyst is actually functioning in a heterogeneous manner or whether it is merely a reservoir for more active soluble gold species, we performed a hot filtration test in the Suzuki–Miyaura cross-coupling reaction of phenyl boronic acid with phenyl iodide after ~50% of the

coupling reaction was completed. The hot filtrates were then transferred to another flask containing  $K_3PO_4$  (3 equiv.) in  $H_2O$  (2 mL) at  $100^\circ C$ . Upon further heating of catalyst-free solution for 6 h, no considerable progress ( $\sim 3\%$  by GC analysis) was observed. Moreover, using AAS of the same reaction solution at the midpoint of completion indicated that no significant quantities of gold were lost to the reaction liquors during the process. ICP result of the used Au NPs@HS-G-PMS nanocomposite catalyst indicate leaching of 1.3% of gold in the Suzuki–Miyaura cross-coupling reaction of phenyl boronic acid with phenyl iodide after the sixth cycle.

**Table 2** Reusability of the Au NPs@HS-G-PMS hybrid in Suzuki–Miyaura cross-coupling of phenyl boronic acid with phenyl iodide<sup>a</sup>

Reaction cycle	1st	2nd	3rd	4th	5th	6th
Yield <sup>b</sup>	93%	93%	93%	91%	91%	90%

<sup>a</sup>Phenyl iodide (1.0 mmol), phenyl boronic acid (1.2 mmol),  $K_3PO_4$  (3.0 mmol), Au NPs@HS-G-PMS (2 mol% of Au),  $100^\circ C$ , 6 h and  $H_2O$  (2 mL).

<sup>b</sup>GC yield, *n*-dodecane was used as an internal standard

Moreover, no appreciable changes in textural properties after six reactions cycles were detected, as clearly evidenced from TEM analysis of the recycled catalyst (Fig. 10). TEM micrographs also indicated no detectable aggregation or agglomeration of Au NPs in the recovered Au NPs@HS-G-PMS hybrid after 6th reaction run. Additionally, TEM micrographs of the recovered Au NPs@HS-G-PMS hybrid showed an increase in size of Au NPs in comparison to the fresh hybrid. There has also been a decrease in the reaction yield about 3% from the first run to the sixth run that indicated the little size dependence on the catalytic activity of Au NPs@HS-G-PMS hybrid.

XPS analysis of Au NPs@HS-G-PMS hybrid after the 6<sup>th</sup> runs revealed the presence high concentration of K and P, which may suggest that some base remains attached to the surface of the solid (Fig. 11). Additionally, the peaks corresponding to Au 4d, C 1s, O 1s, S 2p & 2s and Si 2p & 2s are clearly observed in the XPS full spectrum.

XRD pattern of Au NPs@HS-G-PMS hybrid after the 6<sup>th</sup> runs show in Fig. 12. The diffractions for the Au crystal are still hard to detect. The peak at  $2\theta=53$  degree correspond to acetate foil transmission X-ray powder diffractometer.

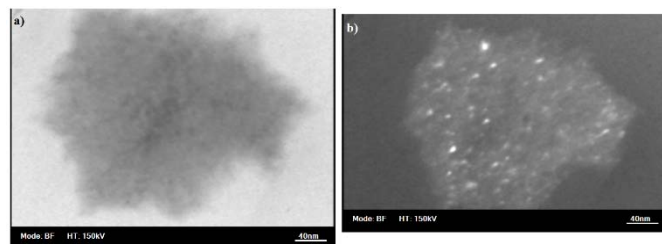


**Fig. 10** TEM micrographs of Au NPs@HS-G-PMS reused after six cycles in Suzuki–Miyaura cross-coupling of phenyl boronic acid with phenyl iodide (a) bright field (b) dark field.

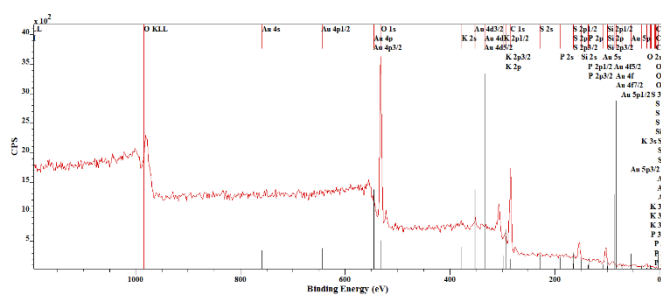


**Fig. 11** Full-range XPS spectrum of Au NPs@HS-G-PMS reused after six cycles.

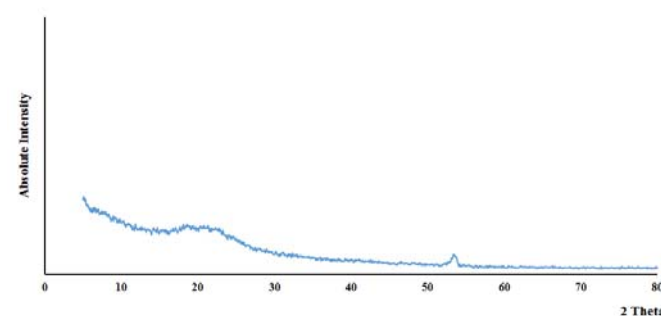


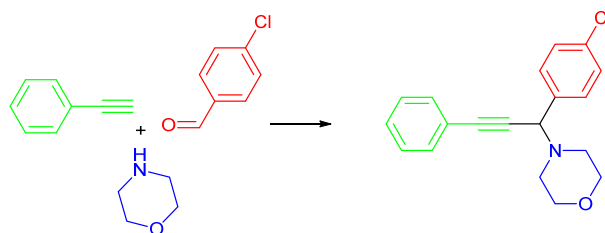
**Fig. 12** XRD pattern of Au NPs@HS-G-PMS reused after six cycles. This XRD pattern was measured on acetate foil.

### The catalytic activity of Au NPs@HS-G-PMS hybrid toward the A<sup>3</sup>-coupling reaction

The three-component coupling of an aldehyde, an alkyne and an amine, commonly called an A<sup>3</sup>-coupling, as MCR, has received much attention in recent years.<sup>29</sup> The resulting propargylamine derivatives are interesting molecules for drug screening, useful intermediates for heterocycle synthesis, and are involved in many different synthetic strategies.<sup>30</sup> For this reason, much effort has been devoted to the development of new alternatives to this extremely useful transformation.

The catalytic activity of the Au NPs@HS-G-PMS hybrid as catalyst was then tested in A<sup>3</sup>-coupling reaction. To optimize the reaction conditions, 4-chlorobenzaldehyde, morpholine and phenylacetylene were tested as model substrates in the presence of various solvents (Table 3). The results indicate that reaction temperature, solvent and loading of Au significantly influence the product yield in the coupling reaction. After several screening experiments with different combinations, the best ones were proved to be Au NPs@HS-G-PMS hybrid (7.5 mol% of Au), 4-chlorobenzaldehyde (1 mmol), morpholine (1.2 mmol), phenylacetylene (1.3 mmol) and  $H_2O$  (3 mL) at  $100^\circ C$  for 24 h.

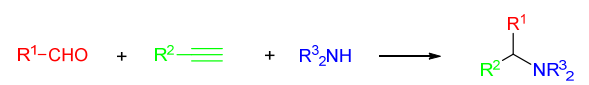


**Table 3** Screening of the A<sup>3</sup>-coupling reaction conditions


Entry	Solvent	Temp. (°C)	Au NPs@HS-G-PMS (mol%)	Yield <sup>b</sup>
1	CHCl <sub>3</sub>	100	7.5	68%
2	CH <sub>3</sub> CN	100	7.5	72%
3	PhCH <sub>3</sub>	100	7.5	51%
4	MeOH	100	7.5	81%
5	H <sub>2</sub> O	100	7.5	93%
6	H <sub>2</sub> O	80	7.5	64%
7	H <sub>2</sub> O	60	7.5	56%
8	H <sub>2</sub> O	100	5	74%
9	H <sub>2</sub> O	100	2.5	49%
10	H <sub>2</sub> O	100	10	94%

<sup>a</sup> 4-chlorobenzaldehyde (1 mmol), morpholine (1.2 mmol), phenylacetylene (1.3 mmol), solvent (3 mL), 24 h; <sup>b</sup> GC yield based on 4-chlorobenzaldehyde

Using the optimized reaction conditions, it was then attempted to expand the scope of benzaldehydes, secondary amines and terminal alkynes applicable to the present A<sup>3</sup> coupling reaction (Table 4). The benzaldehyde bearing electron-withdrawing groups (*p*-Cl and *p*-NO<sub>2</sub>) led to higher yield compared with the benzaldehyde bearing electron donating group (*p*-Me and *p*-OMe) (Table 4, entry 1-3). Moreover, the 4-chlorobenzaldehyde was used in A<sup>3</sup>-coupling with piperidine or pyrrolidine and phenylacetylene (Table 4, entries 6 and 7). Furthermore, by using various substituted phenylacetylenes with substituents that have different electronic properties, different yields of the final products were achieved. The aryl acetylene bearing electron-donating groups (*p*-Me) were more reactive compared with the aryl acetylene bearing electron withdrawing group (*p*-CF<sub>3</sub>) (Table 4, entries 8 and 9), which could be a reflection of the reduced nucleophilicity of the acetylide anion.

**Table 4** Au NPs@HS-G-PMS hybrid catalyzed A<sup>3</sup>-coupling reaction<sup>a</sup>


Entry	R <sup>1</sup>	R <sup>2</sup>	R <sup>3</sup> <sub>2</sub>	Yield <sup>b</sup>
1	4-Cl-C <sub>6</sub> H <sub>4</sub>	Ph	Morpholine	93%
2	Ph	Ph	Morpholine	89%
3	4-Me-C <sub>6</sub> H <sub>4</sub>	Ph	Morpholine	82%
4	4-MeO-C <sub>6</sub> H <sub>4</sub>	Ph	Morpholine	79%
5	4-NO <sub>2</sub> -C <sub>6</sub> H <sub>4</sub>	Ph	Morpholine	98%
6	4-Cl-C <sub>6</sub> H <sub>4</sub>	Ph	Piperidine	96%
7	4-Cl-C <sub>6</sub> H <sub>4</sub>	Ph	Pyrrolidine	77%
8	4-Cl-C <sub>6</sub> H <sub>4</sub>	4-CF <sub>3</sub> -C <sub>6</sub> H <sub>4</sub>	Morpholine	84%
9	4-Cl-C <sub>6</sub> H <sub>4</sub>	4-Me-C <sub>6</sub> H <sub>4</sub>	Morpholine	96%
10	Ph	4-Me-C <sub>6</sub> H <sub>4</sub>	Piperidine	82%

Aldehyde (1 mmol), arylacetylene (1.3 mmol), secondary amine (1.2 mmol), Au NPs@HS-G-PMS (7.5 mol% of Au), H<sub>2</sub>O (3 mL), 100°C and 24 h; <sup>b</sup> GC yield based on aldehyde

The reusability of the Au NPs@HS-G-PMS hybrid was examined in A<sup>3</sup>-coupling reaction of 4-chlorobenzaldehyde, morpholine and phenylacetylene. It was found that the recovery can be successfully achieved in six successive reaction runs (Table 5). ICP result of the used Au NPs@HS-G-PMS hybrid indicate leaching of 4.9% of Au in A<sup>3</sup>-coupling reaction of 4-chlorobenzaldehyde, morpholine and phenylacetylene after the sixth cycle. The comparison between the catalysis reaction using only Au NPs<sup>31</sup> and Au NPs@HS-G-PMS hybrid shows that unsupported Au NPs show sharp drop in activity and delayed reaction time after five cycles (92% in 5 h for the first run to 63% in 18 h for the fifth runs).

**Table 5** Reusability of the Au NPs@HS-G-PMS hybrid in A<sup>3</sup>-coupling reaction of 4-chlorobenzaldehyde, morpholine and phenylacetylene<sup>a</sup>

Reaction cycle	1st	2nd	3rd	4th	5th	6th
Yield <sup>b</sup>	93%	93%	90%	88%	88%	86%

<sup>a</sup> 4-chlorobenzaldehyde (1 mmol), morpholine (1.2 mmol), phenylacetylene (1.3 mmol), Au NPs@HS-G-PMS (7.5 mol% of Au), H<sub>2</sub>O (3 mL) 100°C and 24 h; <sup>b</sup> GC yield based on 4-chlorobenzaldehyde

## Conclusion

In summary, a 2-D hybrid material has been developed by the ultra-small Au NP immobilization on sandwich-like mesoporous silica encapsulated G. The as-prepared Au NPs@HS-G-PMS hybrid exhibited a high catalytic activity for the reduction of 4-NP, the Suzuki-Miyaura cross coupling reaction for a range of aryl bromides and iodides with phenyl boronic acid and A<sup>3</sup>-coupling reaction of aldehyde, alkyne, and secondary amine in water. Moreover, the catalyst was chemically stable and could be recycled for at least six times in the corresponding reaction without reduction in the catalytic activity. Furthermore, the TEM image of the recovered catalyst showed the presence of well-distributed Au NPs on the HS-G-PMS sheets without any aggregation.

## Acknowledgements

We gratefully acknowledge financial support from the Research Council of Shahid Beheshti University.

## Notes and references

<sup>a</sup> Faculty of Chemistry, Shahid Beheshti University, Tehran, Islamic Republic of Iran. E-mail: m-dabiri@sbu.ac.ir; Fax: +98 21 22431661; Tel: +98 21 29903255.

- M. D. Stoller, S. Park, Y. Zhu, J. An and R. S. Ruoff, *Nano Lett.*, 2008, **8**, 3498.
- K. I. Bolotin, K. J. Sikes, Z. Jiang, M. Klima, G. Fudenberg, J. Hone, P. Kim and H. L. Stormer, *Solid State Commun.*, 2008, **146**, 351.
- C. Lee, X. D. Wei, J. W. Kysar and J. Hone, *Science*, 2008, **321**, 385.
- D. Li, M. B. Muller, S. Gilje, R. B. Kaner and G. G. Wallace, *Nat. Nanotechnol.*, 2008, **3**, 101.
- R. X. Huang, X. Qi, F. Boey and H. Zhang, *Chem. Soc. Rev.*, 2012, **41**, 666.
- B. F. Machado and P. Serp, *Catal. Sci. Technol.*, 2012, **2**, 54.
- S. K. Maji, S. Sreejith, A. K. Mandal, X. Ma and Y. Zhao, *ACS Appl. Mater. Interfaces*, 2014, **6**, 13648; S. Yang, X. Feng, L. Wang, K.

- Tang, J. Maier and K. Mullen, *Angew. Chem. Int. Ed.*, 2010, **49**, 4795; Z.-M. Wang, W. Wang, N. Coombs, N. Soheilnia and G. A. Ozin, *ACS Nano*, 2010, **4**, 7437; C. Zhu, L. Han, P. Hu and S. Dong, *Nanoscale*, 2012, **4**, 1641.
- 8 L. Shang, T. Bian, B. Zhang, D. Zhang, L.-Z. Wu, C.-H. Tung, Y. Yin and T. Zhang, *Angew. Chem.*, 2014, **126**, 254.
- 9 L. Wu, J. Wang, H. Sun, J. Ren and X. Qu, *Adv. Healthcare Mater.*, 2013, **3**, 588.
- 10 Y. Fang, Y. Chen, X. Li, X. Zhou, J. Li, W. Tang, J. Huang, J. Jin and J. Ma, *J. Mol. Catal. A: Chem.*, 2014, **392**, 16.
- 11 J. C. Love, L. A. Estroff, J. K. Kriebel, R. G. Nuzzo and G. M. Whitesides, *Chem. Rev.*, 2005, **105**, 1103; A. C. Templeton, W. P. Wuelfing and R. W. Murray, *Acc. Chem. Res.*, 2000, **33**, 27; P. Ghosh, G. Han, M. De, C. K. Kim and V. M. Rotello, *Adv. Drug Deliv. Rev.* 2008, **60**, 1307; C. D. Bain, E. B. Troughton, Y. T. Tao, J. Evall, G. M. Whitesides and R. G. Nuzzo, *J. Am. Chem. Soc.*, 1989, **111**, 321.
- 12 W.S. Hummers and R.E. Offeman *J. Am. Chem. Soc.*, 1958, **80**, 1339; N.I. Kovtyukhova, P.J. Olliver, B.R. Martin, T.E. Mallouk, S.A.Chizhik, E.V. Buzaneva and A.D. Gorchinsky *Chem. Mater.*, 1999, **11**, 771.
- 13 A. Jorio, M. S. Dresselhaus, R. Saito and G. F. Dresselhaus, in *Raman Spectroscopy in Graphene Related Systems*, Wiley-VCH, Berlin, 2011.
- 14 X. Fu, F. Bei, X. Wang, S. O'Brien and J. R. Lombardi, *Nanoscale*, 2010, **2**, 1461.
- 15 A.C. Ferrari and J. Robertson, *Phys. Rev. B*, 2000, **61**, 14095.
- 16 S. G. Leonardi, D. Aloisio, N. Donato, P. A. Russo, M. C. Ferro, N. Pinna and G. Neri, *ChemElectroChem*, 2014, **1**, 617.
- 17 G. Goncalves, P. A. A. P. Marques, C. M. Granadeiro, H. I. S. Nogueira, M. K. Singh and J. Gracio, *Chem. Mater.*, 2009, **21**, 4796; A. Champion, J. E. Ivanecky and C. M. Child, *J. Am. Chem. Soc.*, 1995, **117**, 11807; H. Ko, S. Singamaneni and V. V. Tsukruk, *Small*, 2008, **4**, 1576.
- 18 R. Leppelt, B. Schumacher, V. Plzak, M. Kinne and R. J. Behm, *J. Catal.*, 2006, **244**, 137; H. G. Boyen, G. Kastle, F. Weigl, B. Koslowski, C. Dietrich, P. Ziemann, J. P. Spatz, S. Riethmuller, C. Hartmann, M. Moller, G. Schmid, M. G. Garnier and P. Oelhafen, *Science*, 2002, **297**, 1533.
- 19 S. K. Movahed, R. Esmatpoursalmani and A. Bazgir, *RSC Adv.*, 2014, **4**, 14586; S. K. Movahed, N. F. Lehi and M. Dabiri, *RSC Adv.*, 2014, **4**, 42155.
- 20 M. Kraft, S. Adamczyk, A. Polywka, K. Zilberberg, C. Weijtens, J. Meyer, P. Görrn, T. Riedl and U. Scherf, *ACS Appl. Mater. Interfaces*, 2014, **6**, 11758.
- 21 K. Singh, D. Everett, R. Haul, L. Moscou, R. Pierotti, J. Rouquerol and T. Siemieniowska, *Pure Appl. Chem.*, 1985, **57**, 603.
- 22 R. B. Rakhi, W. Chen, D. Cha and H. N. Alshareef, *J. Mater. Chem.*, 2011, **21**, 16197; B. Nam, H.-J. Lee, H. Goh, Y. B. Lee and W. S. Choi, *J. Mater. Chem.*, 2012, **22**, 3148.
- 23 B. Yu, X. Jiang and J. Yin, *Nanoscale*, 2013, **5**, 5489; Z. Zhai, C. Hu, X. Yang, L. Zhang, C. Liu, Y. Fan and W. Hou, *J. Mater. Chem.*, 2012, **22**, 19122.
- 24 J. Hermannsdörfer and R. Kempe, *Chem. Eur. J.*, 2011, **17**, 8071.
- 25 Y. Wang, K. Wang, J. Zhao, X. Liu, J. Bu, X. Yan, and R. Huang, *J. Am. Chem. Soc.*, 2013, **135**, 4799.
- 26 Y. Choi, H. S. Bae, E. Seo, S. Jang, K. H. Park and B.-S. Kim, *J. Mater. Chem.*, 2011, **21**, 15431; X. Le, Z. Dong, Y. Liu, Z. Jin, T.-D. Huy, M. Le and J. Ma, *J. Mater. Chem. A*, 2014, **2**, 19696.
- 27 Z. Zhang, C. Shao, P. Zou, P. Zhang, M. Zhang, J. Mu, Z. Guo, X. Li, C. Wang and Y. Liu, *Chem. Commun.*, 2011, **47**, 3906.
- 28 N. Miyaura and A. Suzuki, *Chem. Rev.*, 1995, **95**, 2457; J. Hassan, M. Sevignon, C. Gozzi, E. Schulz and M. Lemaire, *Chem. Rev.*, 2002, **102**, 1359; V. Farina, *Adv. Synth. Catal.*, 2004, **346**, 1553; F. Bellina, A. Carpita and R. Rossi, *Synthesis*, 2004, 2419; F.-S. Han, *Chem. Soc. Rev.*, 2013, **42**, 5270.
- 29 V. A. Peshkov, O. P. Pereshivko and E. V. Van der Eycken, *Chem. Soc. Rev.*, 2012, **41**, 3790.
- 30 Y. He, M.-F. Lv and C. Cai, *Dalton Trans.*, 2012, **41**, 12428; X. Tang, J. Kuang and S. Ma, *Chem. Commun.*, 2013, **49**, 8976.
- 31 M. Kidwai, V. Bansal, A. Kumar and S. Mozumdar, *Green Chem.*, 2007, **9**, 742.